Monthly Report (Yamamoto Lab.)

date: 2018.Jun.30
Author: R. Oechslin (M2)

Research theme: **Haptic Feedback Controller with Palm Pressurization**

— Research Plan —

Term \Month	2	3	4	5	6	7	8	9	10	11	12	1
Literature review												
Design PlayStation Controller												
Test PlayStation Controller												
Frequency Response Analysis												
Design Pilot Controller												
Test Pilot Controller												
Theoretical Analysis												
Analyze data and compare												
Write Thesis												

— Work Contents —

1 Introduction

This report is the continuation of the first two reports about the project "Haptic Feedback Controller with Palm Pressurization". The last report has left off ...

2 Theoretical analysis

To come up with a theoretical analysis of the transfer function, a simplifying mechanical schematic has been drawn. This schematic can be seen in figure 1. The equations of motion

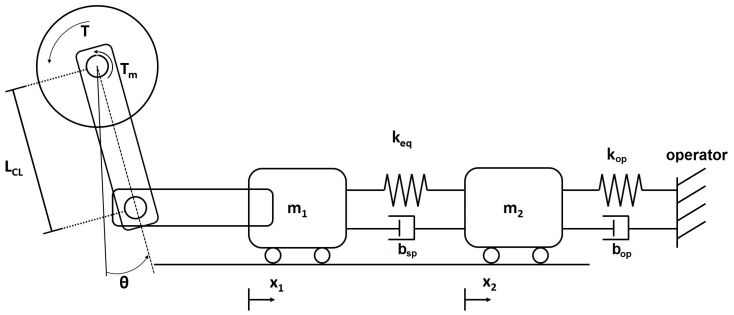

Figure 1: Simplifying mechanical schematic of the actuation system with the stimulator.

can be formulated with the major parameters defined in the schematic. A full explanation of all parameters can be seen in table 2. The variables with subscript 1 refer to the first mass element, the carriage in its guideway, whereas variables with subscript 2 refer to the stimulator, the palm pad. For the motor the subscript m has been used.

Designator	Explanation	Unit
T_m	Motor torque	[Nm]
T	Output torque acting on carriage	[Nm]
θ_m	Motor angle	[rad]
θ	Clamp link angle	[rad]
L_{CL}	Clamp link length	[m]
m_1	Mass of the carriage in its guideway	[kg]
m_2	Mass of the stimulator	[kg]
x_1	Position of the carriage in its guideway	[m]
x_2	Position of the stimulator	[m]
k_{eq}	Equivalent spring constant	[N/m]
b_{sp}	Spring damping coefficient	[Ns/m]
n	Reduction gear ratio	[-]
k_{op}	Spring constant of the operator	[N/m]
b_{op}	Damping coefficient of the operator	[Ns/m]
J_T	Total inertia of mechanical setup	$[kgm^2]$

Figure 2: Setup parameters

Assumptions

First of all, it is important to mention that the transfer function is non-linear, due to the motor angle θ_m that determines the force acting on the carriage c_1. As an initial approach however, this effect has been neglected. More specifically, it is assumed that $\theta \ll 1$ and $\cos(\theta)\frac{T_m}{L_{CL}} = F_{carr}$ becomes $\frac{T_m}{L_{CL}} \simeq F_{carr}$. Here the angle θ is the angle of the lever, pushing the carriage (ie. $\theta_m = n\theta$). Furthermore, there are several types of friction in the system: the intrinsic friction within the motor and its reduction gear, inside the bearings and the carriage in its guideway. Additionally the springs have a non-negligible damping coefficient. In this work the overall friction and the spring damping have been merged and are represented by the friction coefficient b_{sp}. The stimulator also called the palm pad, is not in contact with the controller, but with the operator. To model the damping of the skin of the operator and the friction between the skin and the palm pad, the damping coefficient b_{op} has been introduced. Similarly the spring constant of the operator's skin is modeled by k_{op}.

Spring Constant and Damping Coefficient of the Operator's Hands

The order of magnitude of the two coefficients k_{op} and b_{op} can be found in research papers [Kuchenbecker et al., 2003] [Park et al., 2014] [Speich et al., 2005]. They all indicate parameters varying in the same order of magnitude, namely $k_{op} \simeq 400$N/m and $b_{op} \simeq 5$Ns/m.

Identification of the Spring Damping Coefficient

The damping coefficient of the spring b_{sp} can be found by comparing the theoretical results of the frequency response analysis with the experimental findings. In fact, for the experimental setup, the stimulator has been fully blocked and therefore the operators spring coefficient can be seen as infinitely stiff.

By varying b_{sp} and Bode-plotting the results of the analytical transfer function, the coefficient's order of magnitude can be found. In order to do so, the analytical transfer function has to be identified.

Expected Transfer Functions

The system can be cut into two major transfer functions. The block diagram including these two transfer functions is depicted in figure 3.

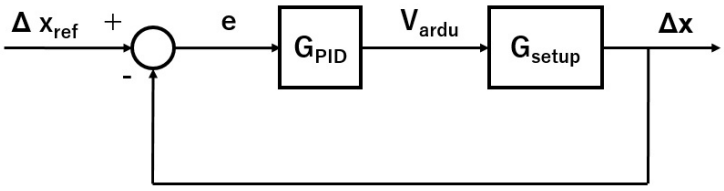

Figure 3: Block diagram with two different transfer functions.

According to this figure one can obtain a transfer function of the following form:

$$F(s) = G_{PID}(s)G_{setup}(s) = \frac{V_{ardu}}{E}\frac{\Delta X}{V_{ardu}} = \frac{\Delta X(s)}{E(s)} \tag{1}$$

where V_{ardu} is the voltage output of the arduino for controlling the motors. Using this form one can calculate the individual transfer functions and finally relate the compression of the springs Δx to the compression given as reference Δx_{ref}, since $\Delta X_{ref}/\Delta x = F/(1+F)$.

PID Transfer Function The transfer function given by the PID controller is very straightforward and can be taken out of any control theory book [Dutton et al., 1997]. Specific for this case is the multiplication factor $K_{\mu m}$ to get from the reference distance in meters to micrometers (to keep the PID gains consistent with the arduino file). Furthermore, an offset has been added $K_{bit-offset} = 128$ to allow for negative armature voltages and lastly the PID value has been converted to the arduino output voltage, where 255 corresponds to 5 V. The transfer function is given in equation 2.

$$G_{PID}(s) = \frac{V_{ardu}(s)}{E(s)} = (K_{\mu m}(K_P + \frac{K_I}{s} + K_D s) + K_{bit-offset})K_{PID2Vardu} \tag{2}$$

Finally, there is also the gain of the amplifier in voltage mode, which converts the voltage of the Arduino into the voltage applied to the motors. This gain is $K_{ampl} = 10\text{Volt/Volt}$. To this voltage an offset voltage of $V_{offset} = -25\text{V}$ is added.

Motor Equations The second transfer function relates the motor torque T_m to the Arduino voltage as well as the output Δx to T_m. Due to the back electromotive force these two parts are related and have to be treated as a whole.

The output torque T_m of the motor can be calculated using the sum of all torques and the conversion parameters intrinsic to the motor.

Similar to the setup and analysis in [Junior et al., 2016] the equations of the motor are given as:

$$L_a\frac{di_a}{dt} + R_a i_a + K_{emf}\dot{\theta}_m = V_a \tag{3}$$

where L_a is the armature inductance, R_a the armature resistance and i_a the armature current of the motor. K_{emf} is the back electromotive force constant also given by the motor. V_a is the armature voltage and θ_m is the angle of the motor shaft.

Furthermore, with Newtons law, the sum of all torques must be zero, or:

$$J_T\ddot{\theta}_m - \frac{k_{eq}L_{CL}}{n}\Delta x - \frac{b_{sp}L_{CL}}{n}(\dot{x}_2 - \dot{x}_1) = T_m = K_\tau i_a \tag{4}$$

Author: R. Oechslin

In equation 4 the parameter J_T stands for the total equivalent inertia of the motor and the clamping link and mass m_1 and K_τ is the proportional current torque gain constant. The moment of inertia can either be calculated as the sum of all inertias seen by the motor shaft, or measured in a simple test.

Analytical Inertia Identification

The total inertia of the system is determined by the inertia of the rotor and gears J_m, the inertia of the clamp link J_{CL} as well as the inertia of the carriage assembly with mass m_1. The last one can be found by simplifying the load to a point mass at distance of the clamp link length L_{CL}, which is given by $J_{carr} = m_1 L_{CL}^2$. The gear box increases the inertia seen by the motor shaft by the square of its ratio n:

$$J_{reflected} = \frac{J_{load}}{n^2} \tag{5}$$

We therefore have a total inertia of:

$$J_T = J_m + \frac{J_{CL}}{n^2} + \frac{m_1 L_{CL}^2}{n^2} \tag{6}$$

where J_{CL} can be calculated by approximating it as a cantilever with an off-center axis of distance $L_{CL}/2$ [1]:

$$J_{CL} = \frac{1}{12} m_{CL}(A^2 + B^2 + 12l^2) \tag{7}$$

where A and B are the width and length respectively.
The calculated total moment of inertia is $J_T = 6.87 \times 10^{-8}\ kgm^2$.

Experimental Inertia Identification

Alternatively, one can approximate the total moment of inertia by applying a constant current on the motor and measuring the acceleration. In this case the traveled distance has been derivated twice to find the acceleration, which results in an amplification of errors. Furthermore, the constant current has been kept very low, (between 20 and 100 A), which led to a slow movement and therefore higher friction impact on the measurements. However, the results are consistent with the theoretically calculated values:

$$J_T = \frac{7.5 \times 10^{-4}}{n^2} = 5.98 \times 10^{-8}\ kgm^2$$

Relating ΔX to θ

The conversion between the angle θ and the distance x can be found by assuming that the horizontal displacement of the carriage is given by $L_{CL} sin(\theta) = x$. For small angles of θ the Taylor expansion gives:

$$L_{CL}\theta \simeq x_1 \tag{8}$$

The output Δx is the compression of the springs and is given by $\Delta x = x_2 - x_1$. For finding x_2 the equation of motion given by Newtons law has to be considered.

$$m_2 \ddot{x}_2 = -k_{eq}(x_2 - x_1) - b_{sp}(\dot{x}_2 - \dot{x}_1) - k_{op} x_2 - b_{op}\dot{x}_2 \tag{9}$$

[1] (2018, June 19th) retrieved from `http://www.orientalmotor.com/technology/motor-sizing-calculations.html`

In the case where the stimulator has been blocked, x_2 has been forced to zero. Using the Laplace transform and equation 9 one finds the expression of x_2:

$$X_2 = -\frac{k_{eq} + b_{sp}s}{s^2 m_2 + b_{op}s + k_{op}} \Delta X \tag{10}$$

Motor and Spring Transfer Function Combining all the equations one can find the final block diagram, which can be seen in figure 4

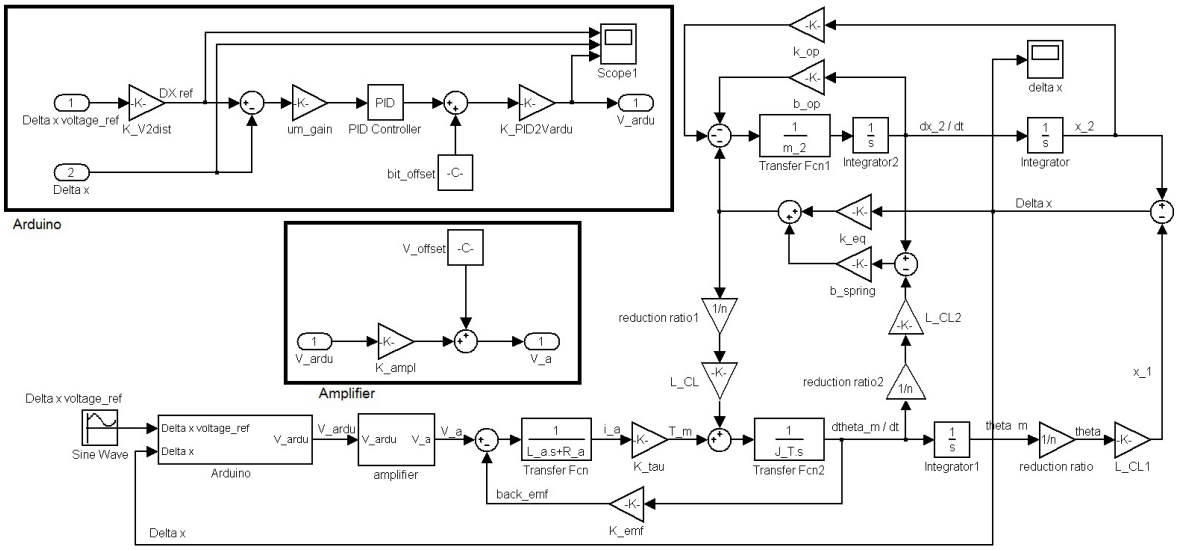

Figure 4: Complete block diagram relating the output Δx to the input Δx_{ref}.

From this diagram and the equations mentioned above, one can obtain the transfer functions that relate the output Δx and input Δx_{ref} as introduced in equation 1, where $\Delta X(s)$ and $\Delta X_{ref}(s)$ are the Laplace transforms of the output and input functions respectively.
It is thus possible to study the frequency response by simulating this setup with the assumptions mentioned earlier.

Main Equations for Analytical Transfer Function

$$\Delta X_{ref} - \Delta X = E \tag{11}$$

$$((K_P + K_D s + \frac{K_I}{s})EK_{\mu m} + K_{bit-offset})K_{PID2Vardu}K_{ampl} + V_{offset} = V_a \tag{12}$$

$$\frac{V_a - K_{emf}\dot{\theta}_m}{L_a s + R_a} K_\tau + F_{coupled} = J_T \ddot{\theta}_m \tag{13}$$

$$F_{coupled} = (k_{eq} + b_{sp}s)\frac{L_{CL}}{n}\Delta X \tag{14}$$

$$\theta_m = \frac{n}{L_{CL}} X_1 = -\frac{n}{L_{CL}}(1 + \frac{k_{eq} + b_{sp}s}{m_2 s^2 + b_{op}s + k_{op}})\Delta X \tag{15}$$

Note that the constant offsets in equation 12 are for pure symmetrical reasons and will cancel each other out, since $K_{bit-offset}K_{PID2Vardu}K_{ampl} + V_{offset} = 0$ and the equation becomes $((K_P +$

$K_D s + \frac{K_I}{s}) E K_{\mu m}) K_{PID2Vardu} K_{ampl} = V_a$. This is the equivalent to a standard PID form with gains K'_P, K'_D and K'_I. In the case of the experimental setup the palm pad has been blocked and therefore x_2 has been forced to be constant. The last equation becomes thus: $\theta_m = -\frac{n}{L_{CL}} \Delta X$.

Analytical Transfer Function

The analytical transfer function has only been calculated for a specific set of spring damping coefficients b_{sp} (ie. 10 uniformly spaced values between 100Ns/m and 1000Ns/m). The gains that have been used are for a P-controller, it was namely $K'_P = 39.2 \frac{V}{mm}$. The simulation result that was closest to the experimental setup can be seen in figure 5 and the corresponding transfer function is:

$$\frac{\Delta X}{\Delta X_{ref}} = \frac{1.23 \times 10^3}{3.24 \times 10^{-6} s^3 + 6.67 \times 10^{-2} s^2 + 8.48 s + 1.23 \times 10^3} \tag{16}$$

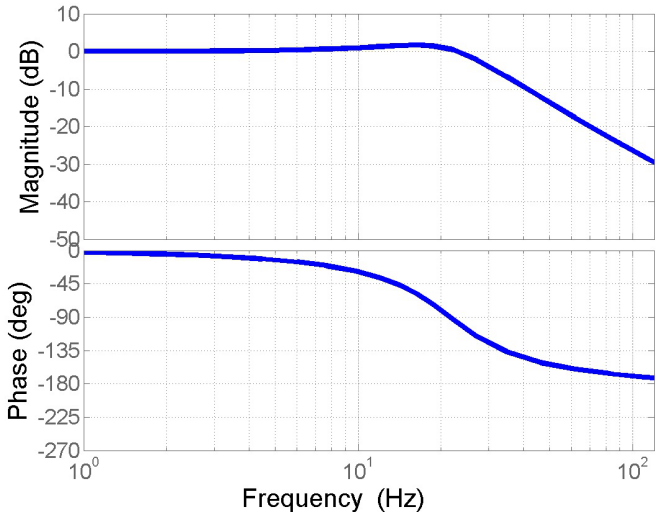

Figure 5: Bode plot of analytical transfer function for $b_{sp} = 400$Ns/m.

As it can be seen in figure 5 there is a constant gain of 1 for lower frequencies and a slight resonance top becomes visible around 20Hz. The phase shift is of around $-180°$ for the tested frequencies, and the lag does not increase more than 45° for the frequencies of interest. Due to the setup constraints, the analytical results of higher frequencies have not been considered.

Motor Comparison

When one goes back to the experimental results where the two motors with different reduction gear ratios have been compared (previous report), one can conclude that the motor with the higher reduction ratio has a higher output force with a tradeoff of speed. Since one of the critical elements of the SEA system is its actuation speed, it is essential to push the boundaries as far as possible. However, the high gain frequency response in the experimental setup starts to drop at much higher frequencies than the actual operating frequency (which is given by the rather slow communication speed between the robot and the control device of $f_{op} \simeq 2 - 5$ Hz.
Due to the fact that even with the stronger reduction gear motor, the springs cannot be compressed to their limits, a higher possible output force has been favored and therefore the stronger motor seems more appropriate.

Experimental PID Tuning

At first, the Ziegler Nichols tuning method has been used to identify the PID gains for the setup. However, due to the rather non-linear behaviour, these gains resulted in a rather poor tracking performance of the reference signal.
Since an educated tuning of the gains is the very core problem of all control engineering, a lot of different approaches exist of finding optimal or sub-optimal gain values. Given the complexity of the setup, it seems reasonable to go for the simple trial and error approach, where the gains are tuned and the tracking performance is tested in real-time. This approach led to the following gain coefficients:

Designator	Explanation	Unit
K'_P	1.6	[V/mm]
K'_I	0.001	[asdf]
K'_D	0.014	[rad]

Figure 6: Trial and error PID tuning.

Analytical PID Implementation

Tracking Behavior

3 Discussion

asdfdf

4 Conclusion

asdf

5 Outlook

faaafaa adsf

References

[Dutton et al., 1997] Dutton, K., Thompson, S., and Barraclough, B. (1997). *The art of control engineering*. Addison Wesley Harlow.

[Junior et al., 2016] Junior, A. G. L., de Andrade, R. M., and Bento Filho, A. (2016). Series elastic actuator: Design, analysis and comparison. In *Recent Advances in Robotic Systems*. InTech.

[Kuchenbecker et al., 2003] Kuchenbecker, K. J., Park, J. G., and Niemeyer, G. (2003). Characterizing the human wrist for improved haptic interaction. In *ASME 2003 International Mechanical Engineering Congress and Exposition*, pages 591–598. American Society of Mechanical Engineers.

[Park et al., 2014] Park, J., Pažin, N., Friedman, J., Zatsiorsky, V. M., and Latash, M. L. (2014). Mechanical properties of the human hand digits: Age-related differences. *Clinical Biomechanics*, 29(2):129–137.

[Speich et al., 2005] Speich, J. E., Shao, L., and Goldfarb, M. (2005). Modeling the human hand as it interacts with a telemanipulation system. *Mechatronics*, 15(9):1127–1142.